January 2010

Nasal flow at High Inspiration Pressures

Kenneth E. Gadow
Worcester Polytechnic Institute

Matthew J. Wetherbee
Worcester Polytechnic Institute

BJS-NF10

Nasal Flow Distribution

A Major Qualifying Project
submitted to Brian J. Savilonis
of the
WORCESTER POLYTECHNIC INSTITUTE
in partial fulfillment of the requirements for the
Degree of Bachelor of Science

by
Kenneth Gadow
Matthew Wetherbee
Date: 13 January 2008

Table of Contents

ABSTRACT

While there are several benefits to nasal medical delivery systems, many questions remain unanswered. Much is still unknown about air flow distribution through the nasal cavity, preventing medical researchers from fully exploiting nasal delivery of vaccines and other medication. Previous studies of airflow through the nasal cavity have been conducted using numerical modeling and measurement devices; there is still very little experimental data visually documenting flow patterns through the nasal cavity.

This project develops and utilizes a system that replicates nasal breathing in order to visually document flow distributions and patterns under a wide range of breathing conditions. It is our hope that this approach and data will prove helpful in future medical research of nasal delivery systems. Our results show that there is a distinct change in flow pattern as pressure increases. This study also demonstrates that a turbinectomy also will change flow patterns and should be accounted for when designing nasal delivery systems.

ACKNOWLEDGEMENTS

Prof. Brian Savilonis- WPI Mechanical Engineering Department – For his continued assistance in the development and completion of this project.

Lincoln Barber- For his help in getting the previous system back in working order. He was a valuable source of information and insight on the apparatus before even before we started getting it to run.

TABLE OF FIGURES

INTRODUCTION –

The nasal cavity and the behavior of airflow through its' different partitions is a very important consideration for medical research and development nasal medical delivery systems.. Currently the majorities of vaccines are administered through injection and are generally very effective in producing a systemic immune response. In nature though, most pathogens prefer to enter the body through the extensive mucus coated surfaces of the gastrointestinal, respiratory, or genitourinary tracts. These surfaces provide a first line of defense for the human immune system. Also, nasal application of a vaccine results in both a systemic and mucosal immune response rather than only the systemic response provided through injection. Thus, the nasal cavity is an ideal location for medication delivery.

Nasal vaccines offer many distinct advantages, including the large absorptive surface area of the nasal cavity. The surface of the nasal epithelium allows for direct medical absorption. It is also a much more comfortable method of vaccination, which is an important consideration when designing vaccines for young children.

While nasal vaccines have many advantages, there is also a very important drawback that must be considered. Mucociliary clearance is an automatic process that takes place within the nasal cavity at a constant pace. The mucus forms a liquid coating of the entire cavity which is moved to the posterior by cilia. Mucociliary clearance is a nonspecific process, so while it moves allergens and other harmful bacteria from the absorptive walls of the nasal cavity, it also rapidly removes medical substances. Under normal conditions, a vaccine will be cleared from the nasal cavity in 21 minutes [12].

Chemical substances have been added to vaccines in order to make them more viscous with hopes of a longer duration on the absorptive tissue. While the vaccines do in fact remain in the nasal cavity for longer with these additives, they have not proven effective in increasing absorption rates. Cilia, a primary mechanism for the mucociliary clearance, are found on the absorptive membranes but not throughout the entire nose. Therefore, the substance is removed from all absorptive surfaces at the same rate with or without the chemical additives. The vaccines with additives tend to pool longer in other areas of the nasal cavity than those without, leading to a longer overall clearance period but with equivalent absorption.

The purpose of this project is to explore and visually document flow distribution through the nasal cavity under different breathing conditions. While much research has been done with computer and numerical modeling, there is very little truly experimental data on the subject. By understanding the different flow patterns, recommendations can be made for extending the duration of nasal vaccines on the absorptive tissue within the nose.

LITERATURE REVIEW

Important topics to understand before reviewing the project are nasal anatomy and function. More specifically, information regarding the surface anatomy of the nasal cavity as well as mucociliary clearance process is explained. In this report, flow patterns are documented through two model nasal cavities, one of which being post-turbinectomy. Medical considerations, the process of a turbinectomy, and studies regarding nasal turbinectomies that have been previously completed are included in the literature review. A basic overview of fluid dynamics is presented in order to familiarize the reader with the necessary scaling considerations when using one fluid to model another. Finally, information about nasal vaccines including current drawbacks is important to understand in order to apply the data and results drawn from this study to medical applications.

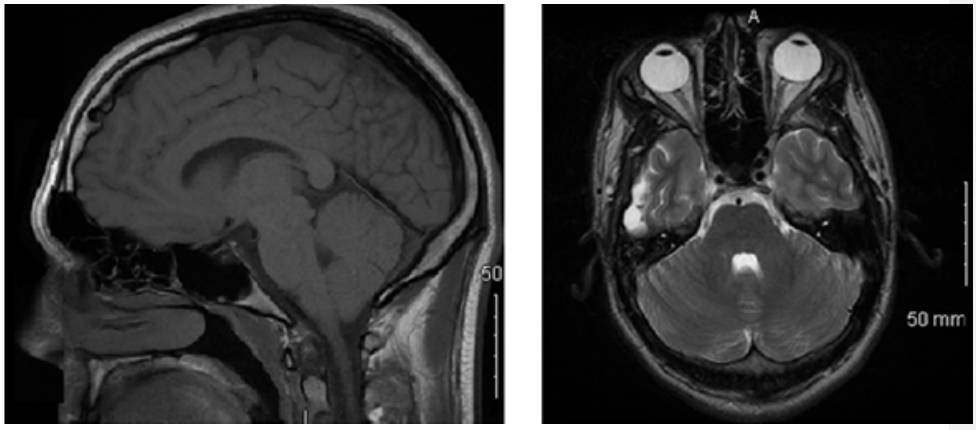

Figure 2: Magnetic resonance Image of head including Nasal Cavity {14}

Nasal Anatomy and Function

While the nose itself only protrudes from the face a few inches, the nasal cavity extends from the nostrils through the skull and into the throat. Figure 1 is a magnetic resonance images of a a live human head that show the nasal cavity both from above and the side.

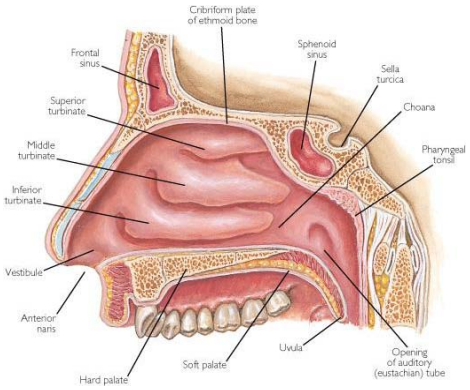

Figure 2: Diagram of turbinate location

The nasal cavity serves many purposes. It is a passage for airflow and the home of the olfactory nerve, the primary source of smell and a secondary taste organ. The nasal cavity is used for breathing primarily during at-rest conditions. When active respiration occurs, the mouth is open and airflow increases, diverting breathing flow away from the nose. Heat transfer also occurs in the nasal cavity, where air is either cooled or heated to within one degree of the body temperature before entering the throat or trachea. Dust is also removed from the air in the nose by small hairs called cilia, and the air is humidified. The structures within the nasal cavity greatly influence airflow. The primary goal of this project is to visually document exactly how alterations in these structures affects air flow. The nasal cavity is split into two symmetrical portions, divided by the nasal septum. The two channels run parallel from front to back of the skull. Each channel has three horizontal outgrowths, called turbinates located on the sides of the cavity. The three are named from top to bottom respectively, the superior turbinate, middle turbinate and inferior turbinate. The surface of the nasal cavity is not homogeneous. Various surfaces are composed of cartilage and other tissue, hair, and bone matter. Each of these

surfaces will alter air flow; giving rise to turbulent eddies in some sections, and laminar flow in others. Figure 2 below displays a cross section of one cavity and labels important physical features. Figure 3 is a frontal cross section of the nose showing the turbinates.

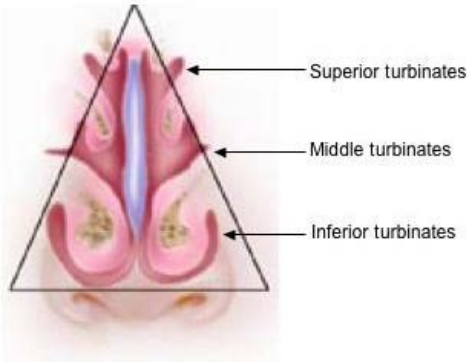

Figure 3: Turbinates from Front [2]

The cross sections of the turbinates are not constant, and give rise to complex air flow through the nasal cavity. The dimensions of the nasal cavity in the turbinate area are about 40 mm high, 1-3 mm wide, and approximately 60 mm deep [2].

Nasal Vaccines and Anatomical Considerations

Intranasal delivery of drugs such as vaccines is becoming a more viable option with emerging research, and poses many benefits over other methods of delivery. Blood can reach peak saturation of substance very quickly due to the permeable mucus membrane in the nose, though there are some marked disadvantages that must be overcome [12]. A special consideration of certain anatomical properties of the nasal cavity is essential when considering nasal vaccines.

The walls of the nasal cavity are not homogeneous; rather it is composed of several types of tissue in different areas. The most important regions of the cavity as far as this study are the three turbinates, because these regions have the highest absorptive properties. The first one third of the cavity, which is inside the physical nose, is covered with squamous and transitional epithelium. The remaining two thirds of the cavity walls are much different. The upper cavity is an olfactory epithelium. We can consider the remainder of this portion a more or less homogeneous psuedostratified and columnar mix epithelium that is more highly ciliated than any other parts of the nasal cavity. Cilia are very small hairs that are constantly in motion. Healthy cilia beat up to 16 times per minute. This beating, along with the fluid mucous membrane that coats the

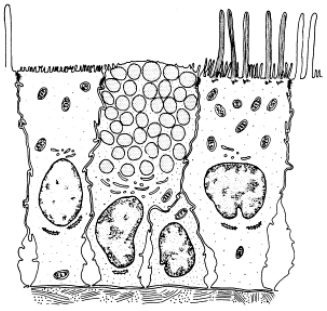

Figure 4: Electron Scan Microscope image of the four types of cells

turbinates, combine to form the automatic immune defense mechanism known as mucociliary clearance [13]. Figure 4 is a depiction of the four types of cells that are found in the nasal cavity.

Mucociliary clearance is one of the few remaining problems for nasal delivery of medical vaccinations that must be solved. The process is a combination of flow of the mucous membrane that coats the nasal cavity and the constant beating motion of the cilia. It takes approximately 15 minutes for a normal human nose to go through one clearance half life, while most current medical nasal applications have a half life of approximately 21 minutes [12].

Current medical research is exploring ways to improve the residual time for the medications, but the problem has yet to be completely resolved. The most successful approach so far has been the addition of substances to the desired medical substances in order to change the viscosity of the solution. Clinical trials have shown that it is the rheological properties rather than the chemical properties of these third party additives that influence the clearance time of the solution. Trials have also demonstrated that nasal sprays with .25% methylcellulose additive have demonstrated decreased clearance times, therefore increasing the half-life of the medication [12]. A more comprehensive understanding of flow patterns under different conditions will aide medical researchers in designing novel nasal delivery systems that incorporate optimal rheological properties with the most effective nasal cavity coating.

Breathing Rates and Flow

To gather effective data, our breathing apparatus must be able to replicate several conditions of human breathing accurately. In order to do so, we must accurately replicate several functional measurements. Total volume, respiration rate, tidal volume, volumetric flow rate, and pressure are the lung parameters that will be taken into consideration. Tidal volume is the lung volume representing the normal volume of air displaced between normal inhalation and exhalation when extra effort is not applied. The total volume measurement relates the volume of air contained in the lungs to time over one breath, and is the maximum of the tidal volume. Volumetric flow rate is defined as the negative of the first derivative of the lung tidal volume, and describes the volume of fluid that enters the lung per given time. The relative pressure measurement is the pressure the fluid exerts inside the nasal cavity. Figure 5 depicts the three time dependent respiration quantities [3].

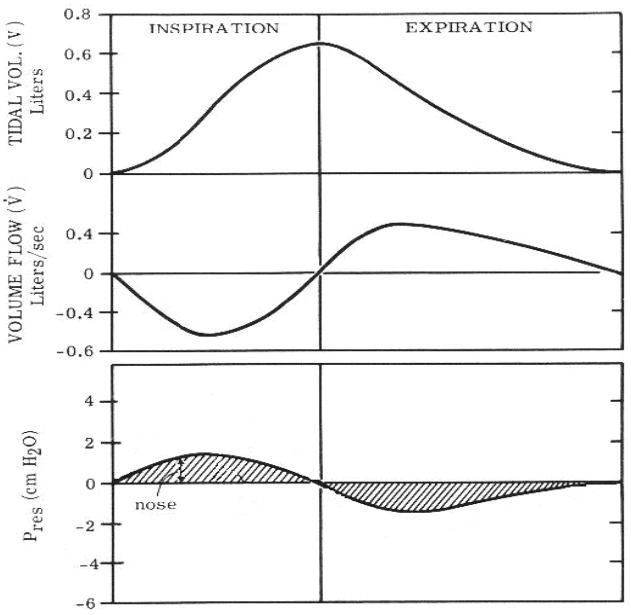

Figure 5: Breathing Rate Graphs

Breathing rates and volumes are dependent upon the overall age and size of the individual. Figure 6 represents the various respiration parameters in proportion to one another, while figure 7 lists several breathing rates based on age.

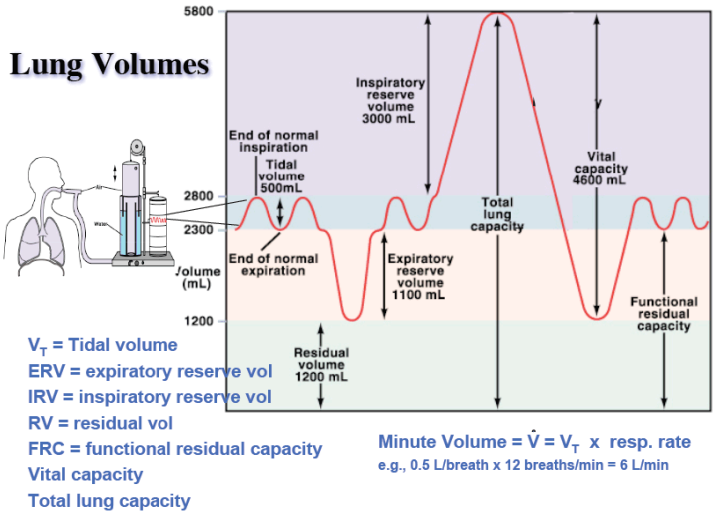

Figure 6: Lung Volumes over Breathing cycle [4]

Typical Breathing Rates		
	Low (BPM)	High (BPM)
Adult	12	20
Teenager	16	25
Preschool	20	30
Infants	20	40
Newborns	44	

Figure 7: Typical BreathingRates vs Age [3]

Total lung volume is a measurement of the maximum capacity of the lung. This parameter is important to our project because it will be represented by the total cylinder volume, rather than the piston displacement through the breathing cycle. The normal lung capacity for a healthy adult ranges from 2.3 to 2.8 liters of air. The average tidal volume is approximately .5 liter.

Minimum tidal volume at rest is referred to as basal tidal volume. The chart displayed below as Figure 8estimates basal tidal volume for an adult based on the parameters of breaths per minute and body weight.

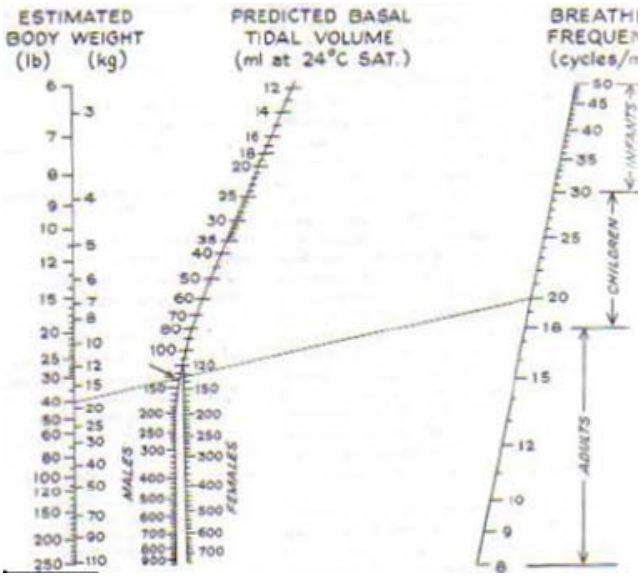

Figure 8: Basal Tidal Volume based on weight and BPM

Figure 9 is a chart that shows various tidal volumes based on the above parameters, adjusted for different age groups.

Typical Breathing Characteristics				
	Weight [lb]	Breathing Rate Low [BPM]	Breathing Rate High [BPM]	Predicted Tidal Volume [L]
Adult	180	12	20	.4-.5
Teenager (14yr)	115	16	25	.24-.3
Preschool (4yr)	36	20	30	.09-.12
Infants (1yr)	22	20	40	.06-.08
Newborns (>1m)	7.5	44	44	.02

Figure 9: Various Tidal Volumes

Pressure

While a study performed at Worcester Polytechnic Institute in 2008 was able to visually document low pressure flow through the nasal cavity using similar methods to this study, there is still very little scientific data and results that explore how flow patterns change based on pressure. Our project's aim is to gather and analyze data under higher pressure breathing conditions in order to create a comprehensive picture of the change in flow pattern based on pressure.

Maximum inspiratory pressure in women is experimentally shown to range from 28 to 66 mm Hg. In men, maximum inspiratory pressure was demonstrated to range between 63 and 97 mm Hg. Both ranges increase as lung volume increases, and all participants were adults considered to be in good health [14].

Nasal Turbinectomy

A nasal turbinectomy is a surgical process that removes part of the turbinate structure (both bone and soft tissue) within the nasal cavity [5]. In some cases, the turbinates can swell and become enlarged due to trauma, allergies, or infection. Generally the result is a partial or complete loss of breathing through the nose. By removing some or all of the turbinates, the airway can be opened and breathing resumed. The procedure is conducted under local or general anesthesia, and is safe and effective at relieving complaints of nasal congestion, snoring, and difficulty breathing [6]. Surgery is conducted by either cauterization, electrocautery, or a microbrider [7]. The surgeon decides whether to remove bone, soft, or all tissue based on individual anatomy.

While the microbrider process is assisted with computer tomography and allows the surgeon to clearly view the location, there is no way yet of knowing exactly what must be removed for the most effective turbinectomies [7].

In some cases, the turbinectomy not only fails to relieve nasal discomfort, but also leaves a patient with a condition called Empty Nose Syndrome (ENS). ENS, also known as wide nasal cavity syndrome is a rare and debilitating iatrogenic syndrome of chronic nasal physiological impairment that results from excessive tissue loss during turbinectomies.

Symptoms include mucosal dryness, areas of squamous metaplasia, congestion, and loss of airflow sensation. These symptoms can lead to grogginess, dizziness, and dispread. Patients claim to have a reduction in quality of life when suffering with ENS [8].

Further review of airflow through the nasal cavity before and after turbinectomies will enhance the surgeon's ability to more accurately remove nasal tissue to ensure the highest level of post-surgery comfort and breathing ability.

Fluid Dynamics

A basic understanding of the fluid dynamic principles at work is important to the reader in order to understand how the alteration in turbinate shape will affect airflow through the nasal cavity. This section covers laminar and turbulent flow, flow separation, and flow parameters important in understanding the overall actions taking place within the nose.

When fluid flows, there are two primary characteristic flow patterns: laminar and turbulent. When a fluid is in laminar flow, smooth layers of the fluid travel at similar speed along similar paths, without frequent mixing. Laminar flow is also called streamline flow. The fluid acts as a series of liquid cylinders in the pipe, where the innermost parts flow the fastest, and the cylinder touching the pipe isn't moving at all. Turbulent flow, on the other hand, is rough. Fluid particles mix rapidly and velocity fluctuates. Eddies and wakes make the flow unpredictable. Turbulent flow creates higher resistance, but also yields higher flux and greater heat transfer rates [9].

Two dimensionless quantities are used to characterize flow: the Reynolds number and the Womersley number. The Reynolds number is an important parameter in equations describing whether flow will be laminar or turbulent. In the case of flow through a circular cross section straight pipe, laminar flow is indicated generally by Reynolds numbers less than 2300. Flows with Reynolds numbers higher than 4000 are considered turbulent, and flow with values in

between are considered transitional [2]. The Reynolds number is defined by the ratio of dynamic pressure (ρu^2) and shearing stress ($\mu u / L$). It allows for accurate comparison of experiment parameters whether using water or air. The speed and type of fluid can easily be switched for more favorable fluids, all while maintaining accuracy. Using the parameters of the human respiratory system, the Reynolds number can be used to find the appropriate flow rate for a model of different size that may breathe a fluid other than air. In this study, the model is a 2:1 scale model of the nasal cavity and will have water flowing through it. The Reynolds number is given by the expression

$$Re_L = \frac{\rho VL}{\mu} = \frac{VL}{v}$$

Symbol	Definition	SI Units
V	Mean fluid velocity	m/s
L	Characteristic length	m
μ	Dynamic Viscosity	$N{\cdot}s/m^2$
v	Kinematic Viscosity	m^2/s
ρ	Fluid Density	kg/m^3

The Womersley number, given by the equation below, is a function of R as an appropriate length scale, ω is the angular frequency of the oscillations, and ν is the kinematic viscosity of the fluid.

$$\alpha = R * \sqrt{\frac{\omega}{v}}$$

It allows for accurate adjustment of the frequency of breathing for a model of different scale. By using the Reynolds and Womersley numbers, we will be able to accurately reproduce human respiration through the nasal cavity using our machine and nasal model [9].

Current research

In recent years there have been a few other groups who have attempted to map out the flow in the nasal passage. There seem to be two main approaches to doing this, both involving computerized modeling and data collection techniques. The first method is a computational fluid dynamics model (CFD) which use purely computer based modeling and equations based on flow rate geometry, and fluid dynamics equations. Model based particle image velocimetry (PIV).is the second measurement tool used in current research.

CFD models have been around for many years now and have gotten progressively better as computer technology has improved. One of the most recent releases was released in 2008 in from Japan. Their objective was to investigate the before and after of a virtual Functional endoscopic sinus surgery, which is a common procedure to relieve chronic rhinosinusitis. They examined 40 individuals who had no history of breathing problems, acute or otherwise, and were able at eliminate all but one, a 40 year old female, based on a series of tests. A CT scan was then modified by nasal experts to clean up the boundaries. These boundaries are then placed into the latest version of fluent software by Gambit. The models were then run using the standard Navier-Stokes equations.[10] These models assumed laminar flow throughout the entire models. It is very difficult to model turbulent flow so most models assume laminar flow throughout.

A second relevant study was published in 2004. It uses PIV technology to map out the velocity vectors at many different points in the nasal passage. Their standard model was an average Korean with no history of nasal or breathing problems. PIV works by passing a coherent light beam through the flow. Mixed into the flow are small particles of a different

material, in this case polyester small polyester particle are scattered in water to produce the required density differences. The double pulse laser is coupled with a CCD camera. This produces two successive readings from which the computer can then determine the direction and distance which the particle has moved. This leads to a velocity vector field from which other flow characteristics can be determined [10].

METHODOLOGY

Specifications

1. Accurate representation of a nasal passage
2. Mechanism to repeatedly mimic breathing pressure and flow rate
3. Mechanism to accurately measure the pressure generated
4. Means of visually recording the flow patterns inside the nasal passage
5. The ability to reset and repeat the experiment.

Design

The apparatus used in this project had a few specific requirements that were very important to consider. First and foremost, it must mimic the flow of air through the nasal cavity. The most important device on the apparatus that achieves this specification is the nasal cavity itself. We were able to obtain a model which was twice the size of an average male nasal passage. The model was created from a CT scan of an adult male which was then three dimensionally printed to form a solid model.

There were many variables to consider when designing to account for the second specification; repeatable pressure and flow rate. More specifically, we need an apparatus which allows accurate repeatable breathing simulation through the nasal cavity while simultaneously producing a clear visualization of the flow.

We chose to work backwards, as the most important part of the project is the visualization of flow through the nasal cavity. Vapors or smoke can be used in an air stream to help visualize the flow patterns; however this presents a few problems. One is would these visual aids stain the inside of the model, thereby limiting the number of experimental runs and damaging the model itself. This leads to a second problem of cleaning the inside of the model. The nasal passage models are small and complex with intricate interior shapes, making any cleaning difficult. After a few tests we determined that smoke was not the best option.

The result of these tests was a conclusion that food coloring in a stream of water was the easiest thing to both keep clean and to see through the model. Red did not stain the models and, because the stream consisted of water, the interior could be cleaned by running the model with clean water or even injecting a solvent if necessary.

As the natural breathing process is an in and out motion, a reciprocating piston seemed like an obvious choice. Some of the previous projects here at WPI had used devices similar to that which we needed, so we used one of these as a starting point for our apparatus. One such device is a computer programmable piston system which had been used as part of an air breathing apparatus. In its original design, the piston moved water into a reservoir which was half full. A cavity model was attached to the top of the reservoir, and the air exiting flowed through the cavity. Below is a schematic of its final design and function.

Design Function

Our final design was based on the previous MQP's computer controlled sled piston design. Below is a picture of the motor side of the machine.

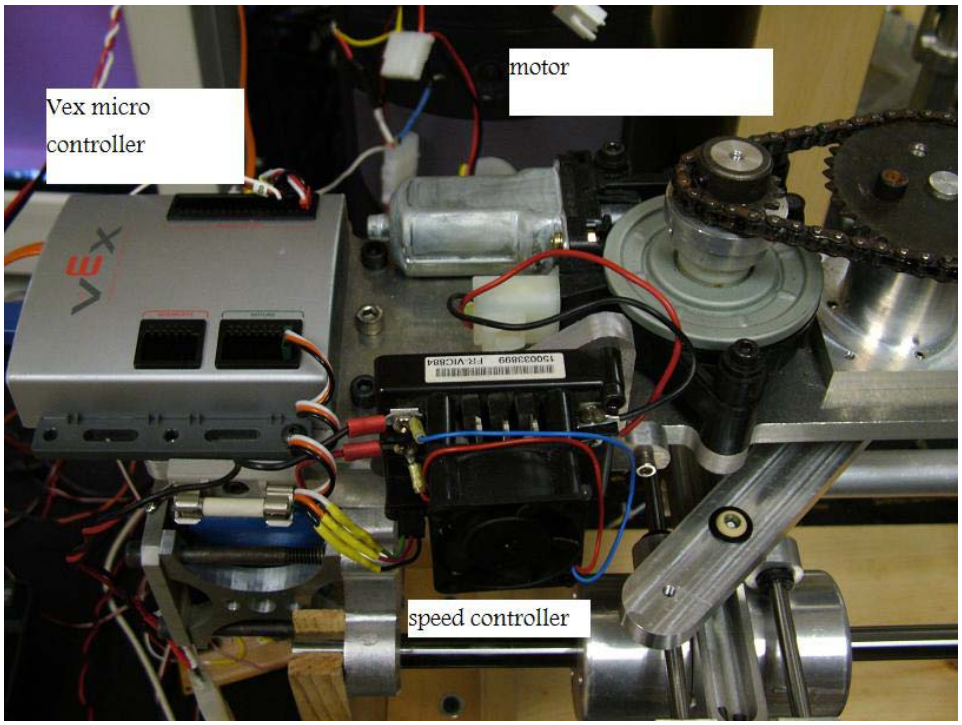

Figure 10: Diagram of electrical components on the apparatus

The Vex micro controller is programmed via the computer in the lab. The only controllable variable is that of motor torque with the value of 127 being zero and 255 being the maximum; the values 127 through 255 are arbitrary units provided through Easy C. This is sent to the speed

controller which regulates the amount of current being drawn by the motor and determines the power output of the motor. The larger sprocket is attached to the shaft and arm which pushes the piston. This in turn regulates pressure and volume flow rate through the nasal passage, which is attached to the nasal passage by a large tube. Water flows from the piston, through the large tube, through the nasal passage, and into a large clear reservoir.

Figure 11: Image of normal nasal cavity connected for breathing

Converting the System to Run Water

In order to determine the requirements of the machine we must convert all of our standard data to use with water through dimensionless analysis. For our analysis the volume flow rate is of lesser importance, however we used Reynolds number (see Equation 1) to obtain a relationship between flow rates Q for use later, and to ensure that the numbers obtained are on the correct order of magnitude of those expected. More important for our evaluation is the use of Euler's constant (see Equation 3) to equate the pressure of water to that of air.

Equation 1: Reynolds number

$$Re = \frac{(4 * Q)}{\pi * d * v}$$

Equation 2: Reynolds number Dimensional Analysis

Formatted: Subscript

$$\frac{(4 * Qn)}{\pi * dn * va} = \frac{(4 * Qm)}{\pi * dm * vw}$$

Qn= flow rate in normal nose Qm= flow rate in model nose

See Appendix 1for complete calculations

Qm = Qn x .12971

Equation 3: Euler's constant

$$E = \frac{P}{\rho * vf}$$

Equation 4: Euler's constant dimensional analysis

$$\frac{Pa}{\rho a * vfa} = \frac{Pw}{\rho w * vfw}$$

See appendix A for complete calculation

Pw = .8722 x Pa

One important number for our analysis if the maximum pressure generated by the average human lung because this is the dictates the maximum amount of air which can flow through the nasal passage. Based on prior studies and our own informal tests in the lab we concluded this pressure to be approximately 85 mmHg. Our informal test consisted of a human subject breathing through a tube connected to a pressure gage at maximum intensity,

These numbers are all based on the actual human subjects; therefore the numbers must be converted to water using the results of Euler's dimensional analysis. The result is an absolute test maximum of 87 mmhg. Tests done by us using the previous group's apparatus revealed this to be a plausible test setting.

Improvements and Final Design

The decision to use portions of a previous MQP presented many obstacles. The prior project was never actually finished, nor did the machine perform as planned. The base and piston were still in the original lab disassembled, however the controlling electronics and motor were not. After meeting with one of the previous project members we had a good idea of the parts necessary to both improve performance and modify the device for our specific needs.

Once all the items were assembled and able to be manually run, another problem which the previous group encountered became quite clear. The entire apparatus buckled and shook while running, quite violently at times, breaking the piston tube. After looking at the original design and testing that apparatus ourselves we determined the cause to be a negative tolerance within the piston tube not allowing free motion through the stroke. The previous group had attempted to remedy this with lubricants but had little success. Our solution was to use a slightly smaller O ring which turned the slight negative tolerance to a virtual zero tolerance. This coupled with a silicone based lubricant resolved both problems.

The next step was modifying the cavity and tank to circulate water through the model instead of air. Our second and final design accomplishes a few things with relatively minor modification. Firstly the model is in open air, making visual documentation of the processes inside easier. During our tests we found the motor to be a bit weak when attempting to push a large volume of water, so secondly, having the reservoir above the model assisted inspiration. Finally, the plastic cup at the front could be easily changed between models.

The previous group had also used a position sensor and a pressure sensor in order to correctly mimic the natural breathing curve. The position sensor can be used as is; however the pressure sensor, though very accurate, can only sense very low pressure. In our case the pressure does not need to be measured precisely since we are not trying to mimic an entire specific pattern, but rather we are only trying to visually compare what happens inside the nasal cavity as pressure is varied. We therefore decided to use a simple manual gauge to indicate pressure inside the passage.

Programming

With the apparatus in working order, a program needed to be developed to keep the simulated respiration consistent with that found in other studies. This was done on a trial and error basis, with the bulk of the emphasis being on the initial inspiration burst as this is the current accepted method for the administration of nasal medication. We use EasyC to program the VEX micro controller which uses a speed controller to control the torque provided by the motor. The program specifications, a sample run, the VEX specifications, and the motor specifications are listed in Appendix C.

Data Collection

For our data collection we used the two resin models obtained, one of which has had a partial turbinectomy. We set out to see not only the flow patterns which emerge from a high pressure inspiration, but also to see the effect of a partial turbinectomy on these flow patterns. As stated in detail in the previous sections, the common practice of a partial turbinectomy removes part of the inferior turbinate. This will undoubtedly cause some difference in the flow pattern, the question is; does this make the application of vaccines and medication more effective, less effective, or even potentially dangerous.

We started with the post surgery model and preformed a rapid inspiration test at pressures varying between 10 and 100 mmHg. We varied the pressure by increasing or decreasing the flow rates. This was done by retracting the piston at various speeds. Dye was injected into the water approximately 1cm in front of the nostrils. 1/2cc was injected prior to the breath, and then a constant stream of dye continued to be injected into the system as the breath took place.

The first observation when comparing this rapid inspiration to the normal breath is that a large percentage of the flow bypasses the lower and middle passages and is channeled through the upper portion of the nasal passage. Going over the data and comparing it to that of a normal breath we see that the volume flow rate is approximately ten times that of a normal breath. This is to be expected as we only use a small portion of our lung capacity when breathing at a normal rate.

RESULTS

During the data collection phase of this study, we used two distinctly different nasal cavity models. One was a normal nasal cavity from a male adult, while the other was from a male adult that had received a turbinectomy. Our aim was to document flow pattern changes under a range of breathing conditions, as well document the effects of a turbinectomy on flow patterns under the same range of breathing conditions. The removal of tissue from the cavity will undoubtedly alter the flow pattern, and the focus is whether or not this altered flow is significant enough to warrant additional considerations of nasal delivery devices for people who have received a turbinectomy.

We started with the post surgery model and performed rapid inhalation tests at pressures varying between 10 to 100 mmHg. The first observation when comparing this rapid inspiration to the normal breath is that a large percentage of the flow bypasses the lower and middle passages and is channeled through the upper portion of the nasal passage. We devised a way to quantify this by visually analyzing what percentage of the flow goes through the different portions of the nasal cavity. Each half of the cavity was divided into four subsections; the uppermost portion and the superior, middle, and inferior turbinates (see Appendix C). By analyzing piston displacement over time with videos of the piston movements corresponding to each breath condition, we found that the volumetric flow rate of our maximum force inhalation is approximately ten times that of a normal breath (see Appendix D). This was anticipated as we only use a small portion of our lung capacity when breathing at a normal rate (tidal volume). Internal velocity rises sharply until the pressure reaches 45mmHg, at which point the velocity levels off until around 65mmHg, at which point it again rises. Many of the studies including our

own, found that 65mmHg corresponds to the maximum inspiration pressure an adult male can produce. Moving on to the normal nose, the same procedure was followed as above. The values on the x axes of the graphs represent motor speeds, which are converted to pressure values in Appendix D. For example, a motor speed of 140 generated a pressure of 8 mmHg, while 160 generated 48 mmHg. The y axis values represent percentage of flow distribution. The results regarding the relationship between pressure and velocity were similar. The significant difference between the two nasal cavities is flow distribution over the entire range of pressures. In the normal nasal cavity, much more flows through the inferior turbinate with the general distribution being much more even amongst the three turbinates. The flow distribution changes are clear in the pictures, which show inhalation flow through both nasal cavities at 45 mmHg. Our data produced clear trends for the percent distribution of flow through each one of the turbinates under different pressures. In a normal nose, we found that as pressure increased flow to the four different stated partitions was as follows.

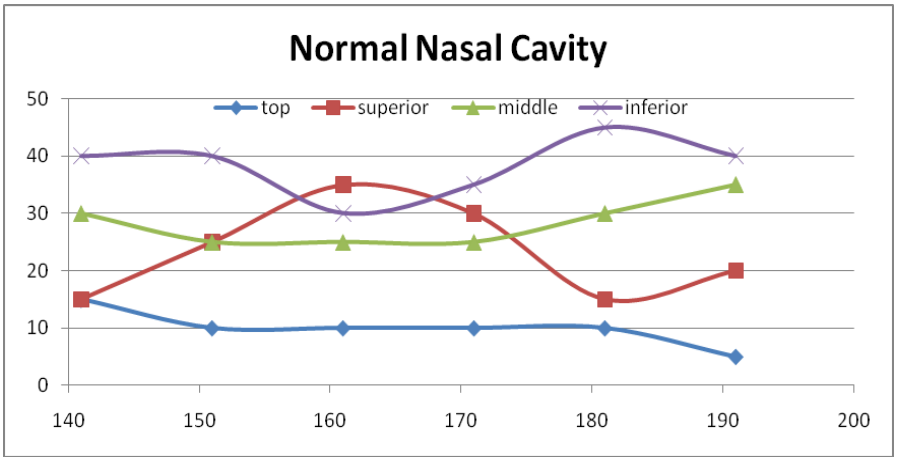

Figure 12: % Flow Distribution as a function of pressure

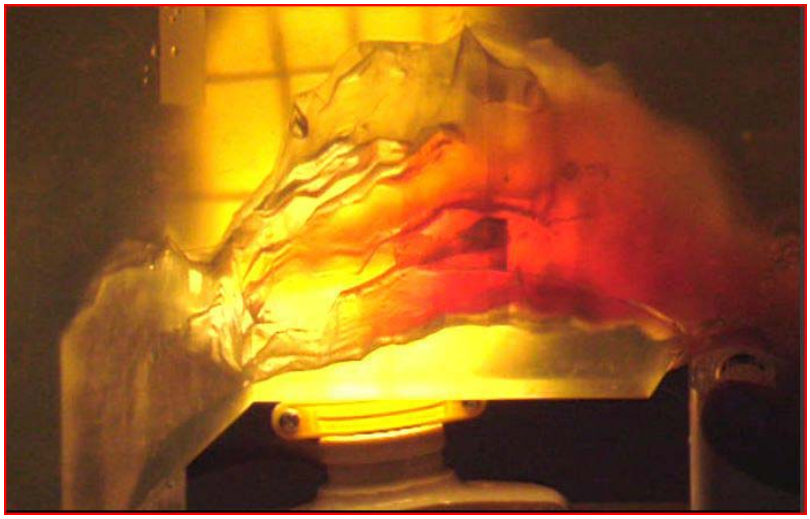

Figure 13: Flow through normal nasal cavity P=45 mmHg

As pressure increases from the low end of the spectrum to the high end the following happens:

- distribution to uppermost portion gradually dropped from 15% to 5%
- distribution to superior turbinate rose sharply from 15 to 35 but fell back to 15 and ended at 20% at maximum inhalation pressure
- distribution to middle turbinate oscillated between 25 and 35 but had no significant trends
- distribution to inferior turbinate drops from 40% to 30% then rose steadily to 45% at max inhalation pressures.

In the post-surgery nasal cavity, the trends were markedly different. Most significantly, the inferior turbinate received the lowest flow rates across the spectrum of conditions post-turbinectomy, while in a normal nose it received a high rate of flow across the spectrum. These more drastic changes of flow distribution are evident in figure 14 below. The photograph of flow through the post surgery cavity at 45 mmHg shows the lack of flow through the inferior turbinate (figure 15).

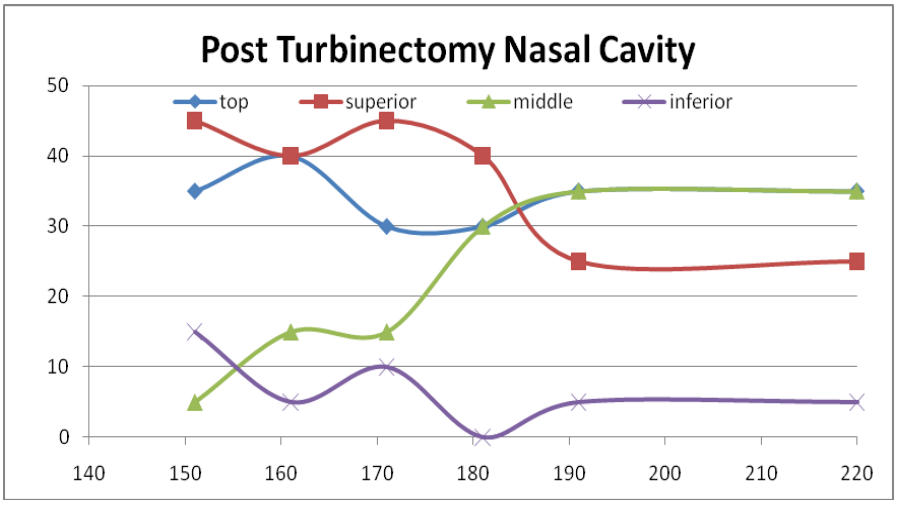

Figure 14: % Flow Distribution in post-turbinectomy nasal cavity

Figure 15: Flow through post-turbinectomy nasal cavity at 45 mmHg

CONCLUSIONS

Through our data collection we have found the flow patterns in pre and post turbinectomy to be very different. To generalize, the post operation nasal passage allows a much higher flow through the upper nasal passages than does the normal nose. This is significant because the inferior turbinate is the largest and has the most surface area; hence it also has the highest absorptive properties. Though the study is not comprehensive enough to confidently make medical conclusions, this data does support the claim that people who have received a turbinectomy should be careful not to inhale with high intensity levels when using nasal medical delivery systems. The altered distribution of medication may lead to a higher rate of mucociliary clearance which decreases the effectiveness of the substance.

We can conclude with confidence that the flow distribution through the three turbinates significantly changes based on pressure. The normal nasal cavity showed an average change of 5% flow distribution across the spectrum and the largest spread experienced by any one subsection was a 20% distribution from maximum to minimum flow distribution. The highest disparity measured from minimum to maximum experimental pressure was 10% in any one subsection.

On the other hand, the average flow distribution changes seen over the spectrum in a post-surgery nose were 15%; three times the levels experienced in the normal cavity. Highest disparity experienced from minimum to maximum distribution in any one region was measured to be 30% and coincided with the highest level of disparity from minimum to maximum pressure.

The goal of this project was to visually document flow patterns under different breathing conditions, as well as note the effects of a turbinectomy on flow patterns. In conclusion, flow patterns do in fact vary based on breathing conditions, and a turbinectomy experimentally led to a much less predictable flow distribution over the spectrum of pressures. We would recommend further exploration of the effects of varied breathing conditions on flow distribution across the entire spectrum. It has potential to make significant improvements of the understanding of nasal flow conditions and can lead to improved nasal delivery systems for vaccinations and other medical substances in the future.

RECOMMENDATIONS FOR FUTURE ENDEAVOURS

The main recommendation that we can make to any future attempts to perform similar studies is to use the same basic concept we used, but with a total reevaluation of the individual components and cylinder dimensions.

Basically every electronic component should be much more reliable in the future if the true goal of the project is to produce results. We had several electronic issues. A power supply died, the vex microcontroller died, the originally intended pressure sensors were unable to function at the specified range, and the motor was not powerful enough to simulate the entire range of breathing conditions. Above all else, a motor with at least twice the power would be an essential upgrade to this project. Higher torques would allow for a slower stroke rate, allowing a wider range of simulated breathing conditions.

There are several geometric design considerations important for future like endeavors. We used a cylinder and piston with a stroke length and circumference predisposed. In order to more readily represent a wide spectrum of breathing conditions, the piston and cylinder should be redesigned. An adjustable stroke length would be a marked improvement, along with a narrower cylinder. Because of the complex scaling involved in modeling air with water, a smaller bore, longer stroke piston-cylinder assembly with stroke adjustments is recommended.

We feel that the concept of a reciprocating piston pumping water through a three dimensional model is a good approach to this problem, but the equipment should be much better in order to facilitate a higher level of data collection in such a short period of time.

WORKS CITED

1. photo taken from:

http://www.hunterian.gla.ac.uk/collections/anatomy/students_projects/nasal/images/Fig1_thumb.jpg

2. Keyhani K., Scherer, P. W., and Mozell, M. M. "Numerical simulation of airflow in the human nasal cavity." *Journal of Biomedical Engineering*, Vol. 117 (1995): 429-41.

3. Fenn, W.O., and Rahn, H. Handbook of Physiology: Respiration. Washington: American Physiological Society, 1964.

4. "Lung Volumes" photo taken from

http://mcb.berkeley.edu/courses/mcb136/topic/Respiration/SlideSet1/Resp1.pdf

5. http://www.rhinoplasty4you.com/breathing_problems.htm

6. http://brianhumphreysmd.com/PDFs/Inferior%20Turbinectomy.pdf

7. Turbinectomy [homepage on the Internet]. . 2002. Available from:

8. Rice DH, Kern EB, Marple BF, Mabry RL, Friedman WH. The turbinates in nasal and sinus surgery: a consensus statement. Ear Nose Throat J. 2003;82(2):82-84.

9. http://www.engineeringtoolbox.com/laminar-transitional-turbulent-flow-d_577.html

10. Guanxia Xiong, Jiemin Zhan, Kejun Zuo, Jianfeng Li, Liangwan Rong, Geng Xu. Numerical flow simulation in the post-endoscopic sinus surgery nasal cavity. Med Boi Eng Compt (2008).

11. **S** K Kim1 and S K Chung. An investigation on airflow in disordered nasal cavity and its corrected models by tomographic PIV. INSTITUTE OF PHYSICS PUBLISHING. Meas. Sci. Technol. **15** (2004) 1090–1096

12. Marttin, E et al. Nasal mucociliary clearance as a factor in nasal drug delivery.Advanced Drug Delivery Reviews vol. 29 13-38 1998. Elsevier Science. 1998

13. Mygind, N & Dahl, R. Anatomy, physiology and function of the nasal cavities in health and disease. Drug Delivery Reviews. Vol 29 3-12. Elsevier Science. 1998

14. photo donated by a personal acquaintance of Ken. Name not included for the sake of skull anonymity.

Appendix A: Scaling Mathematics

The Reynolds number must be calculated in order to scale volumetric flow rate. The calculations are below:

$$\mathrm{Re}_d = \frac{4 \times Q}{\pi \times d \times \nu}$$

$$\frac{4 \times Q_N}{\pi \times d_N \times \nu_{Air}} = \frac{4 \times Q_M}{\pi \times d_M \times \nu_W}$$

$$Q_M = \frac{4 \times Q_N}{\pi \times d_N \times \nu_{Air}} \times \frac{(\pi \times d_M \times \nu_W)}{4}$$

$$d_M = 2 \times d_N$$

$$Q_M = \frac{Q_N}{d_N \times \nu_{Air}} \times (2 \times d_N \times \nu_W)$$

$$Q_M = \frac{Q_N}{\nu_{Air}} \times (2 \times \nu_W)$$

$\nu_{Air} = 1.52 \times 10^{-5}$ m^2/s at 21.1°C (70 °F)

$\nu_W = 9.817 \times 10^{-7}$ m^2/s at 21.1 deg C (70 deg F)

$$Q_M = \frac{Q_N}{\nu_{Air}} \times (2 \times \nu_W)$$

Eurler's Constant must be calculated in order to properly scale the pressure due to the different properties of air and water. The calculations are below:

$$E_u = \frac{P}{\rho \times V_F}$$

$$\frac{P_A}{\rho_A \times V_A^{\,2}} = \frac{P_W}{\rho_W \times V_W^{\,2}}$$

$$V_F = \frac{Q}{A}$$

$$V_A = \frac{Q_N}{A_N}$$

$$V_W = \frac{Q_M}{A_M} = \frac{Q_N \times .12917}{4 \times A_N}$$

$$\frac{P_A}{\rho_A \times \left(\frac{Q_N}{A_N}\right)^2} = \frac{P_W}{\rho_W \times \left(\frac{Q_N \times .12917}{4 \times A_N}\right)^2}$$

$$\frac{P_A}{\rho_A} = \frac{P_W}{\rho_W \times \left(\frac{.12917}{4}\right)^2}$$

$$P_W = \frac{P_A}{\rho_A} \times (.001043 \times \rho_W)$$

$\rho_A = 1.1934$ kg/cu m

$\rho_W = 997.97$ kg/cu m

Appendix B: Equipment Specifications

vEx Microcontroller

Inputs and Outputs	
Battery input	7.2 volts nominal, 6 to 9 volts min/max input range
Battery Type	6 AA batteries (not included) or VEX Robotics Power Pack
Interrupt inputs	6
Digital I/O	16 max with no Analog, Each can be input or Output (shared with Analog)
input Impendence	Analog/Digital - The input consists of a 470K pull-up to +5V and a series resistance of 1K to the uP. Interrupts - The input consists of a series resistance of 1K to the uP.
Analog inputs	16 max with no Digital, 10-bit resolution (shared with Digital)
Digital/Analog as inputs	3 dB bandwidth of 150 kHz, weak pull-up of 470k-ohms to 5.0 volts, need 0.0 to 0.6 volts for a low and 4.0 to 5.0 volts for a high
Interrupts as inputs	3 dB bandwidth of 150 kHz, weak pull-up of 47k-ohms to 5.0 volts, need 0.0 to 0.6 volts for a low and 4.0 to 5.0 volts for a high
Digital/Analog Interrupts as Outputs	As outputs these ports can drive an open circuit to 0.6v or lower for a low and 4.0 volts or higher for a high. They can drive a 1 mA load to 1.6v or lower for a low and 3.0 volts or higher for a high.
PWM Outputs	As outputs these ports can drive an open circuit to 0.6v or lower for a low and 4.0 volts or higher for a high. They can drive a 1 mA load to 1.0v or lower for a low and 3.6 volts or higher for a high.
Digital input Freq.	50 KHz (typical)
Analog input Access	10 µSec
Motor Output	8 PWM Outputs for motors or servos, refreshed every 18.5mSec

Serial Ports	TTL (115Kb) - Serial Port and TX/RX on Digital/Analog port
Pinout	Digital/Analog, Interrupts, Motor Outputs: Outside pin (closest to the controller edge) Ground Digital/Analog, Interrupts: Center pin (or middle pin) + 5 Volts, 1 Amp Max combined total from all pins Motor Outputs: Center pin (or middle pin) + Battery Power, 4 Amps Max combined total from all pins Digital/Analog, Interrupts, Motor Outputs: Inside pin (furthest from the controller edge) Signal / Control line
User Programmable Microcontroller	
User Microcontroller	Microchip PICmicro® PIC18F8520
Processor Speed	10 MIPS (Million Instructions Per Second)
Variable Space	1800 bytes + 1024 bytes EE2
Program Space	32K
Programming	PIC C
Programming Tools	Microchip MPLAB IDE or easyC
Erase/Write Cycles	100,000
Data Retention	> 40 years
General Features	
Size (W x L x H)	4.5" x 3.9" x 1.1"
Weight	0.28 lbs.
Battery	7.2V Rechargeable Nickel Cadmium batteries - NiCd
Charging	Recharge when battery voltage $\leq$ 7.1V, full charge 7.8V typical
Battery	7.2V Rechargeable Nickel Cadmium batteries - NiCd
Current Draw	62 mA - Controller & Receiver min, 5mA to 2A per Motor, 20mA to 1.5 A per Servo

Victor 884 Speed Controller

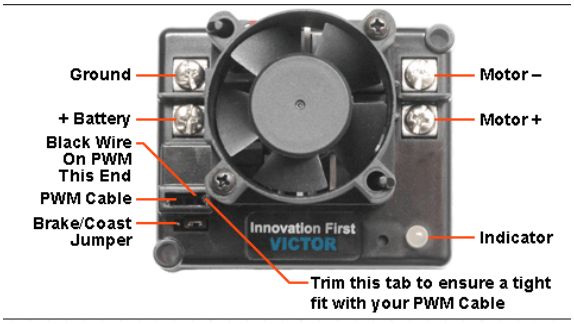

Control Signal	Standard R/C Type PWM (Pulse Width Modulation)
Operating Voltage	6V to 15V
Maximum Current	40A continuous
Minimum Throttle	3%
Power Connector	6-32 Screw Terminals
Signal Connector	Use a standard non-shrouded PWM cable (3 wires)
Typical Application	Power one motor with variable speed forward, reverse, or off
Weight	0.25 lbs

Denso Window motor

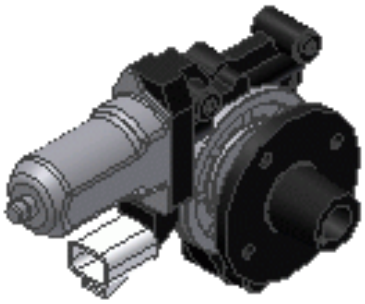

Speed (rpm)	Torque (N m)	Torque (in lbs)	Current (A)	Power (wt)	Efficiency	Heat (wt)
0	10.600	93.818	18.6	0.0	0.00%	223
6	9.893	87.560	17.5	5.9	3.00%	204
11	9.187	81.312	16.3	11.0	6.00%	185
17	8.480	75.054	15.2	15.3	8.00%	167
23	7.773	68.797	14.1	18.7	11.00%	150
29	7.067	62.548	12.9	21.2	14.00%	134
34	6.360	56.291	11.8	22.9	16.00%	119
40	5.653	50.033	10.7	23.7	19.00%	104
46	4.947	43.785	9.5	23.7	21.00%	91
52	4.240	37.527	8.4	22.9	23.00%	78
57	3.533	31.270	7.3	21.2	24.00%	66
63	2.827	25.021	6.1	18.7	25.00%	55
69	2.120	18.764	5.0	15.3	25.00%	45
75	1.413	12.506	3.9	11.0	24.00%	35
80	.707	6.257	2.7	5.9	18.00%	27

86	.000	0.000	1.6	0.0	0.00%	19

Appendix C: Flow Distribution Data

Appendix C

	Post surgery			
torque	Top %	Superior %	Middle %	Inferior %
151	35	45	5	15
161	40	40	15	5
171	30	45	15	10
181	30	40	30	0
191	35	25	35	5
220	35	25	35	5

		pre surgery		
torque	Top %	Superior %	Middle %	Inferior %
141	15	15	30	40
151	10	25	25	40
161	10	35	25	30
171	10	30	25	35
181	10	15	30	45
191	5	20	35	40

Appendix D: Flow rate calculations and scaling

Pre surgery torque	volume flow rate liters/sec	internal velocity top ft/sec	pressure mmHg	time evaluated sec
141	1.02	0.6588	8	0.25
151	1.367	1.85	22	0.16667
161	1.5	1.94	48	0.116667
171	1.67	2.25	61	0.133333333
181	2.07	3	78	0.1
191	2.19	3.5	97	0.066666667

post surgery torque	volume flow rate liters/sec	internal velocity ft/s	pressure mmHg	time evaluated sec
141	0.603	0.625	10	0.433333333
151	1.167	1.37	28	0.166666667
161	1.89	1.8	45	0.133333333
171	2.07	1.91	56	0.166666667
181	2.24	2.06	61	0.166666667
191	2.41	2.58	78	0.1
220		2.7	94	0.133333333